Random laser of dye-injected holey photonic-crystal fiber

Yaado Yonenaga and Ryushi Fujimura*
Interdisciplinary Graduate School of Science and Engineering, Tokyo Institute of Technology, Nagatsuta, Midori-ku, Yokohama 226-8502, Japan

Masayuki Shimojo
Department of Materials Science and Engineering, Shibaura Institute of Technology, Koto, Tokyo 135-8548, Japan

Atsushi Kubono
Department of Electronics and Materials Science, Shizuoka University Johoku, Naka-ku, Hamamatsu, Shizuoka 432-8561, Japan

Kotaro Kajikawa†
Interdisciplinary Graduate School of Science and Engineering, Tokyo Institute of Technology, Nagatsuta, Midori-ku, Yokohama 226-8502, Japan

(Received 2 March 2015; published 14 July 2015)

Random laser action is observed in a holey photonic-crystal fiber (PCF) whose holes are filled with a solution of 4-(dicyanomethylene)-2-methyl-6-(4-dimethylaminostyryl)-4H-pyran laser dye. Although the holes of the PCF are periodically ordered, the laser action does not stem from the Bragg reflection due to the periodic order. A detailed investigation demonstrates that random laser action is the only possible mechanism for the laser oscillation. The PCF is a promising quasi-two-dimensional random laser platform that is convenient for investigating the mechanism of random laser oscillation.

DOI: 10.1103/PhysRevA.92.013824 PACS number(s): 42.55.Zz, 42.55.Mv

I. INTRODUCTION

Random lasers have been extensively investigated in the last decade [1–15]. Scatterers distributed randomly in a gain medium provide coherent or incoherent feedback, and the laser oscillation condition is obtained without using any artificial laser cavity. The feedback is ascribed to strong multiple scattering by the scatterers. Dielectric particles, semiconductors, metallic particles, liquid crystals, and so on are typically used as scatterers.

Holey photonic-crystal fibers (PCFs) have many holes in their cladding. The core is surrounded by a silica cladding in which the holes are periodically separated with two-dimensional order. Because the holes in a silica cladding cause the effective refractive index (RI) to be lower than that of silica, light is confined in the core and propagates within the fiber. The PCF is typically used for white light generation and nonlinear optics [16–18]. It is also used for sensors and other optical devices because of its unique structures [19,20],

In this paper, we report random laser action in a holey PCF in which the holes are filled with a laser dye solution. Although the holes are periodically ordered, the observed laser action is not ascribed to Bragg reflection. The holes act as scatterers, and the random laser condition is created as a result of multiple scattering by the holes. PCFs have the following advantages: (1) The size distribution of the PCF holes is narrow, (2) a variety of scattering conditions can be examined using solutions with different RIs, and (3) the laser emission is confined mainly to the plane of incidence because of the PCF structure. Therefore it is a promising quasi two-dimensional random-laser platform that is convenient for investigating the mechanism of random laser oscillation.

II. EXPERIMENTAL

The main PCF used was a SM-25 index-guiding holey fiber, purchased from Newport. The cross-sectional structure of SM-25 is depicted in Fig. 1(a). According to the data sheet [21], the silica core is surrounded by holes and the PCF is covered with an acrylate polymer layer (thickness $t = 71\ \mu$m) to support the PCF mechanically. As shown below, the acrylate layer does not contribute to the laser emission, and was not removed, because the RI of silica is close to that of acrylate. Optical microscopy was used to determine the diameter of the holes, $d = 5\ \mu$m; the core diameter, $D_1 = 25\ \mu$m; and the diameter of the PCF, $D_2 = 268\ \mu$m. The holes are hexagonally ordered and the period is evaluated to be $\Gamma = 8\ \mu$m. We also used a SM-8 PCF, the cross-sectional structure of which is depicted in Fig. 1(b). The dimensions of the SM-8 are $D_1 = 8.5\ \mu$m, $D_2 = 245\ \mu$m, $d = 3\ \mu$m, $\Gamma = 6\ \mu$m, and $t = 60\ \mu$m. The PCFs were cut approximately 20 mm long, and the holes were filled with a DCM solution. A glass capillary with an inner diameter of 250 μm was used for a reference.

The laser dye used was 4-(dicyanomethylene)-2-methyl-6-(4-dimethylaminostyryl)-4H-pyran (DCM), which was purchased from Sigma-Aldrich. It was dissolved in solution at a concentration of 0.15 wt %. Different solvents were used to vary the RI: 2-ethoxyethanol acetate (2EA) (Tokyo Chemical Industry), toluene, dichloromethane, and mixtures of toluene and dichloromethane at different mixture ratios. We used capillary force to fill the holes with the dye solution by immersing one side of the PCF in the solution.

*Current address: Utsunomiya University.
†Corresponding author: kajikawa@ep.titech.ac.jp

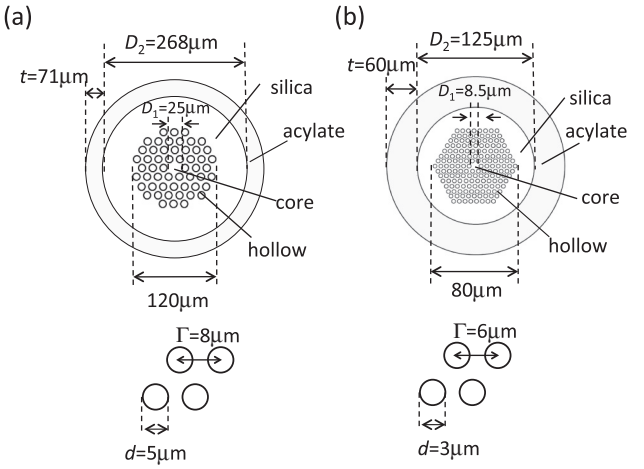

FIG. 1. Cross-sectional drawings of PCFs used in this study: (a) SM-25 and (b) SM-8.

The optical geometry for probing the laser emission is depicted in Fig. 2. The light source was a Nd:YAG laser (LS-2135, LOTIS TII) running at 532 nm (second-harmonic light) with a pulse width of 7 ns at 10 Hz. The pump light was focused with a cylindrical lens. The spot was 0.5 mm wide and 10.5 mm long. The backscattered light was conveyed to a USB-4000 spectrometer (Ocean Optics) using a bundle optical fiber of 400-μm diameter, after the pump light is removed using a notch filter at 532 nm. The spectral resolution of the spectrometer was 0.2 nm. The spectrum was captured for 100 ms to observe one emission spectrum for one excitation pulse, and ten spectra were averaged.

III. RESULTS AND DISCUSSION

Figure 3(a) shows an emission spectrum from the SM-25 PCF and that from the glass capillary, both filled with a 0.15 wt % DCM in a 2EA solution. The excitation intensities were 6.9 and 9.5 mJ/mm^2, respectively. The incident light polarization was along the long axis of the PCF [transverse magnetic (TM) polarization]. The spectra are averaged ones over ten shots. Each spectrum taken for one shot is stable and almost identical. Although sharp emission peaks are observed in the spectrum from the PCF, only broad fluorescence emission without any sharp peaks is observed in that from the

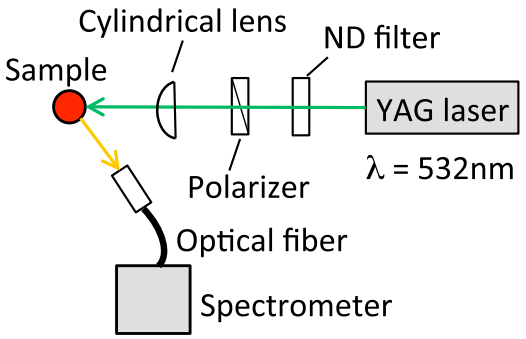

FIG. 2. (Color online) Optical setup for probing laser emission. ND: neutral density.

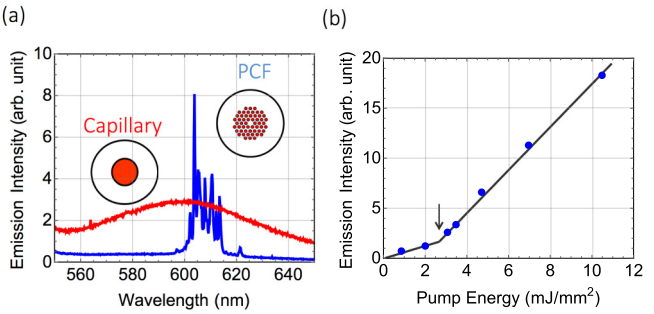

FIG. 3. (Color online) (a) Emission spectra from the dye-injected SM-25 PCF and capillary. (b) Emission intensity and bandwidth (FWHM) of the emission as a function of incident energy.

capillary. Figure 3(b) shows the emission intensity is plotted as a function of pump energy. The emission intensity is the average of the peaks over the wavelengths 600–620 nm. The threshold energy is 2.5 mJ/mm^2. We show the emission spectra from a PCF with an acrylate layer [Fig. 4(a)] and that from the PCF without the acrylate layer [Fig. 4(b)]. Although the emission intensity differs somewhat, the spectra are essentially the same in that the spectra consist of many spikes within the wavelengths 600–620 nm. This indicates that the acrylate layer does not contribute to the laser oscillation.

Figure 5(a) shows the emission spectrum from a SM-8 PCF filled with 0.15 wt % DCM in a 2EA solution. Many laser emission peaks are observed, similar to the spectra from the SM-25 PCF. The emission intensity as a function of the pump energy is plotted in Fig. 5(b). The threshold energy is 1.5 mJ/mm^2, which is similar to that of the SM-25 PCF.

To investigate the laser oscillation mechanism, we examined the lasing conditions at the different RIs of the solvent. The solvents are 2EA (RI: 1.35), toluene (RI: 1.51), dichloromethane (RI: 1.44), and mixtures of toluene and dichloromethane at different mixture ratios (RI: 1.45–1.49) [22]. The PCF material is silica. Although the RI of the silica of the PCF is not provided in the data sheet, the RI of silica ranges from 1.45 to 1.52 at a wavelength of 600 nm. The excitation threshold of the laser emission is plotted as a function of the solution RI in Fig. 6. Because lasing occurs when the RI of the solution is less than that of the silica, it cannot be due to the whispering gallery mode (WGM) within the hole [23–25]. This is because the RI of the cylindrical cavity must be greater than that of the surrounding medium to achieve WGM conditions.

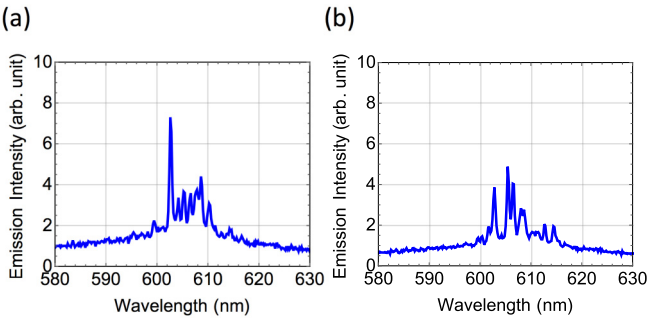

FIG. 4. (Color online) Emission spectra from SM-25 (a) with and (b) without embedded acrylate layer.

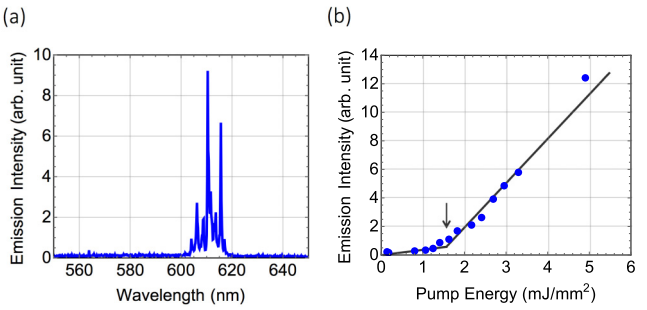

FIG. 5. (Color online) (a) Emission spectra from the dye-injected SM-8 PCF and dye-injected capillary. (b) Emission intensity and bandwidth (FWHM) of the emission as a function of incident energy.

In addition, laser emission was observed even when the RIs of the solutions were close to that of silica. This means that the lasing does not stem from the scattering due to the difference between RIs of the PCF and the solution. The mechanism will be discussed later.

Further, the PCF was rotated and the emission spectra were recorded. The hole has a sixfold rotation symmetry around the long axis of the fiber, and the measurements were made at the rotation angles of 0 to 60°. Figure 7 shows the emission spectra at different rotation angles, at an excitation energy of 19 mJ/mm^2. The peak positions and the intensity scarcely vary with the rotation angle. This means that the laser emission does not stem from the Bragg reflection of the ordered holes.

To investigate the effective volume for laser emission, we selectively injected the DCM solution into various numbers of holes N, where the DCM solution is filled (below we call the dye-filled holes "active holes") and measured the laser emission. The holes on one side of the PCF were partially plugged, by smearing high-viscosity epoxy resin (glue) on one side of the PCF, using a home-made micromanipulator. The dye solution was injected into the holes using capillary force by immersion of the other side of the PCF in the solution. The solution did not fill in the holes that were plugged by the resin on the other side of the PCF because of air in the holes. Only the unplugged holes were filled with the solution. The plugged holes are difficult to specify in the microscope images from the glue side, and we cut the PCF after filling it with the

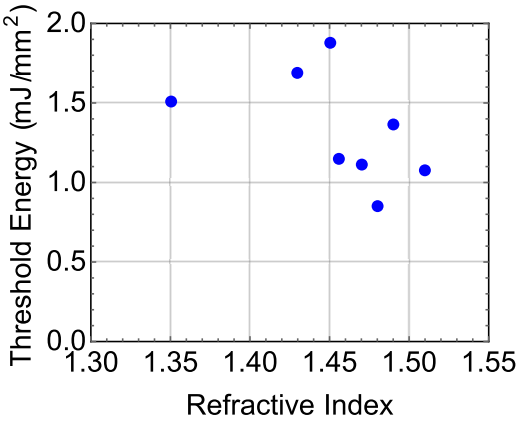

FIG. 6. (Color online) Threshold as a function of RI of the solution.

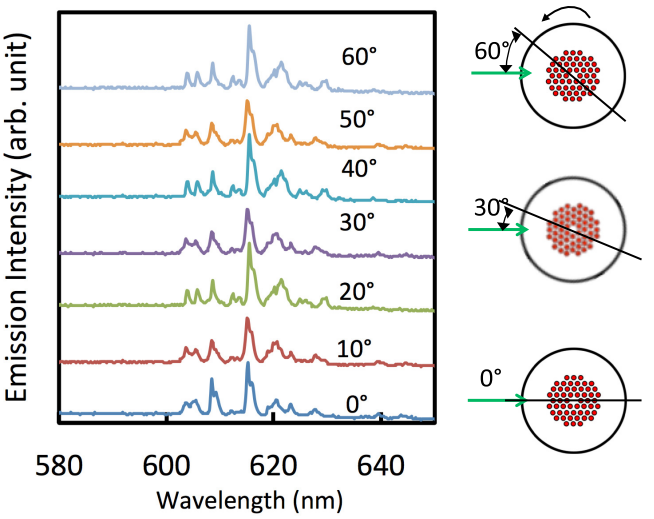

FIG. 7. (Color online) Emission spectra as a function of the rotation angle.

solution and observed the cross section to evaluate the number of the active holes N using an optical microscope.

Table I summarizes the emission status and the threshold pump energy at different N; cross sections of the PCF are also shown, where active holes are indicated by red circles for TM-polarized excitation. In these samples, the active holes are assembled. The corresponding emission spectra are shown in Fig. 8. No emission was observed at $N = 8$, where the active holes are too few to produce an observable signal. Emission was observed with spectral narrowing at $N = 14$. The full width at half maximum (FWHM) of the spectrum is 20 nm whereas that of the fluorescence spectra from weak excitation is approximately 90 nm. The narrowing is due to amplified spontaneous emission (ASE) at a large pump energy. Laser emission with many spikes occurs above $N = 22$, where the number of active holes is sufficient for random laser oscillation. This is supported by the fact that the threshold pump energy decreases with increasing N.

TABLE I. (Color online) Emission status and threshold energy of laser oscillation for PCFs having various numbers of active holes N.

Cross section	N	Emission	Threshold (mJ/mm^2)
	48	Laser oscillation	2.3
	30	Laser oscillation	6.5
	22	Laser oscillation	39
	14	Narrowing	
	8	No signal	

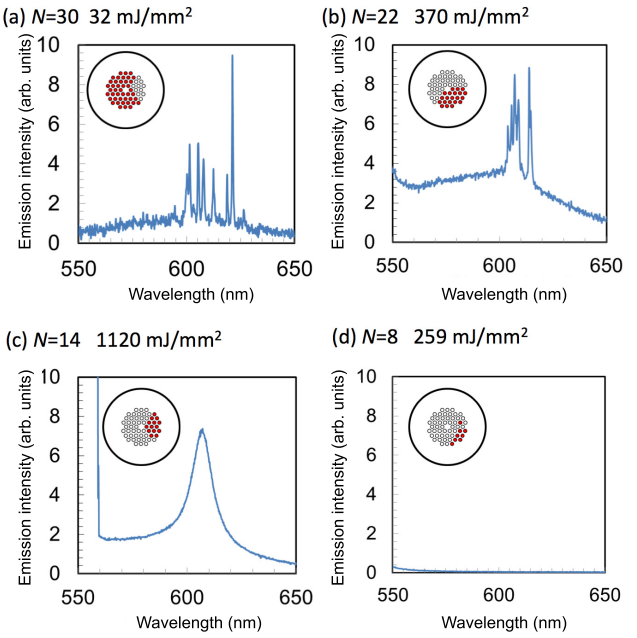

FIG. 8. (Color online) The spectra of the PCF listed in Table I. The number of active hollows and excitation energy are given.

TABLE II. (Color online) Emission status and threshold energy of laser oscillation for PCFs with different active-hole patterns.

Cross section	N	Emission	Threshold (mJ/mm^2)
	48	Laser oscillation	2.3
	16	Narrowing	
	8	Narrowing	
	10	Fluorescence	
	16	Narrowing (TM)	
		Fluorescence (TE)	

Table II summarizes the emission status and the threshold pump energy at different N values, where the active holes are arranged in patterns, for TM and transverse electric (TE) polarizations. A micromanipulator (SS-QP-2RLH, Micro Support)

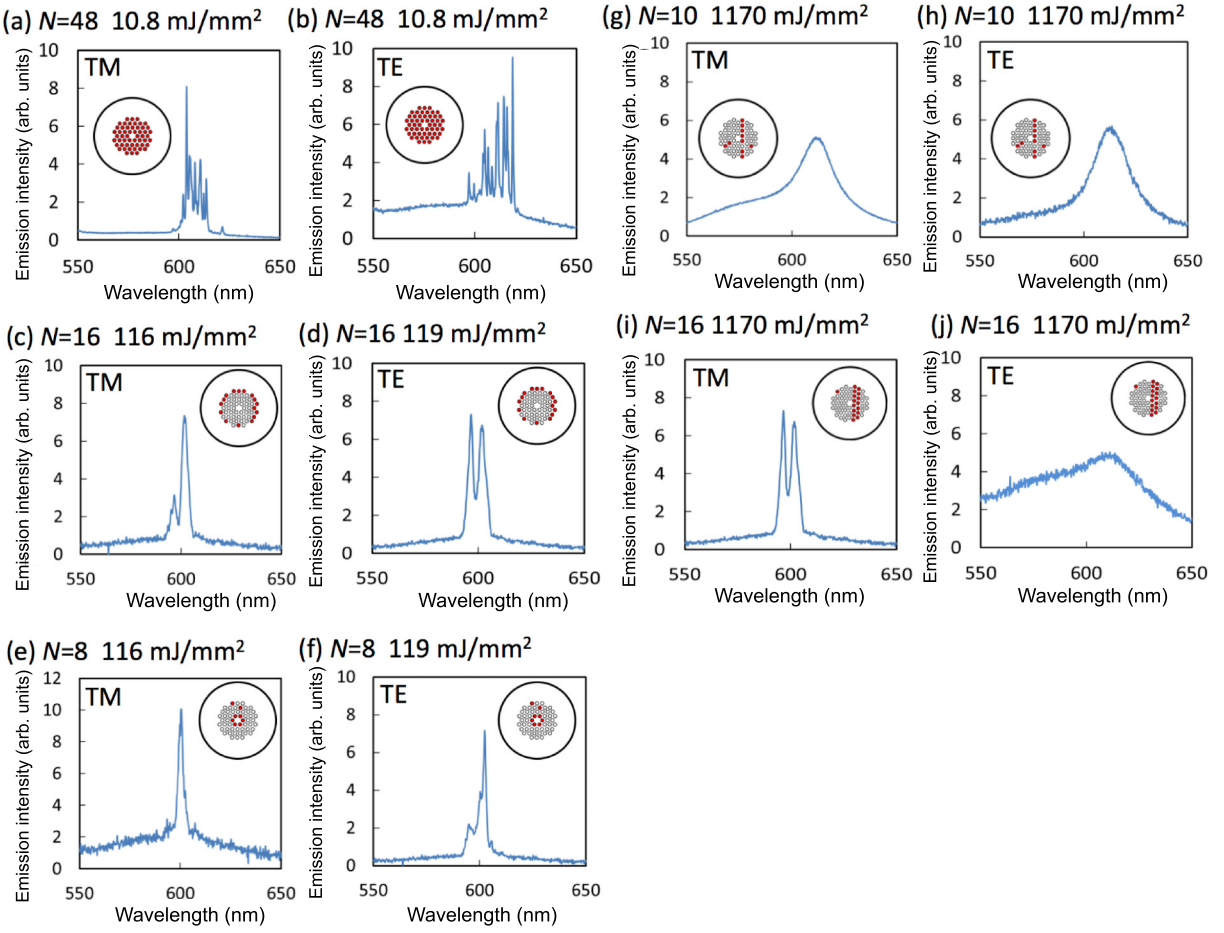

FIG. 9. (Color online) The spectra of the PCF listed in Table II. The number of active hollows and excitation energy are given.

was used, instead of the home-made manipulator, because better resolution is needed. The results are similar for both polarizations, unless otherwise specified. The corresponding emission spectra are shown in Fig. 9. When the active holes are aligned in a circular pattern, spectral narrowing is observed even at $N = 8$. In contrast, when active holes are aligned linearly, very little spectrum narrowing occurs. The assembled pattern of the active holes is necessary for laser oscillation.

The results discussed above indicate that the laser oscillation is not due to WGM or a Bragg cavity. The WGM mode along the periphery of the PCF cannot be the mechanism because the dye-filled holes are located in the central region of the PCF. Therefore we conclude that random lasing is the only possible laser oscillation mechanism, even though the PCF platform is periodic.

One phenomenon is still unexplained: the scattering occurs even when the RIs of the scatterers are close to that of the surrounding medium. To explain this behavior, we need to consider the imaginary part of the RI of the DCM solution. The DCM dye has little absorption at the laser oscillation wavelengths, but has a gain at these wavelengths. The scattering problem from a gain medium can be calculated by considering that the DCM solution has a negative imaginary RI [26–28].

Consider a cylinder with a complex RI of m in a medium with a RI of n_0. The real part is n and the imaginary part is κ. So $m = n + \kappa i$. The cylinder diameter is set to be 5 μm. The difference between the real parts of the RIs of the cylinder and the surrounding medium, Δn, is defined as $\Delta n = n - n_0$, where the RI of the surrounding medium is set to be $n_0 = 1.45$. The length is infinite. The details of the calculation are given in Appendix A. Figure 10(a) shows the scattering intensity, $\Delta I_s(\phi)$ at a position 8 μm apart from the center of the cylinder, calculated for a cylinder with $\Delta n = 0.001$ and $\kappa = 0$ when a plane wave with an intensity of unity and TM polarization is incident on the cylinder along the x axis (arrow). It is plotted as a function of the azimuthal angle ϕ from the direction of the incident light. The position 8 μm corresponds to the distance between the holes of the SM-25 PCF. $\Delta I_s(\phi)$ is maximum at $\phi = 180 \pm 20^\circ$. Then $|\Delta I_s(\phi)|$ is about 0.015.

Figure 10(b) shows the scattering intensity calculated at $\Delta n = 0$ and $\kappa = 0.001$. In this case, only slight absorption and no difference in the real part of the RI are considered. $|\Delta I_s(\phi)|$ is maximum at $\phi = 180 \pm 30^\circ$ and the maximum is about 0.008. Figure 10(c) shows the scattering intensity calculated at $\Delta n = 0$ and $\kappa = -0.001$, where the cylinder has a gain without any index difference. The large $|\Delta I_s(180^\circ)|$ is due to transmission light and does not contribute the random laser oscillation. $|\Delta I_s(\phi)|$ is maximum at $\phi = 145$ and 215°, and the maximum is about 0.003. These calculated results indicate that scattering may occur even when the difference in the real part of the RI is absent. The condition $\kappa = -0.001$ corresponds to a gain of $\sim$300 cm^{-1}, which is a possible value for DCM [29–34].

In these cases the scattering intensity is on the order of 10^{-3}–10^{-2}. Although the scattering efficiency is small, the random laser oscillation may occur. There are a few reports on a random laser in a nematic liquid crystal (NLC) [8–11], in which the director of NLC molecules is thermally fluctuated. Scattering originates in the spatial RI distribution in the NLC medium due to the thermal fluctuation. We evaluated the spatial distribution to be on the order of 10^{-3}, according to

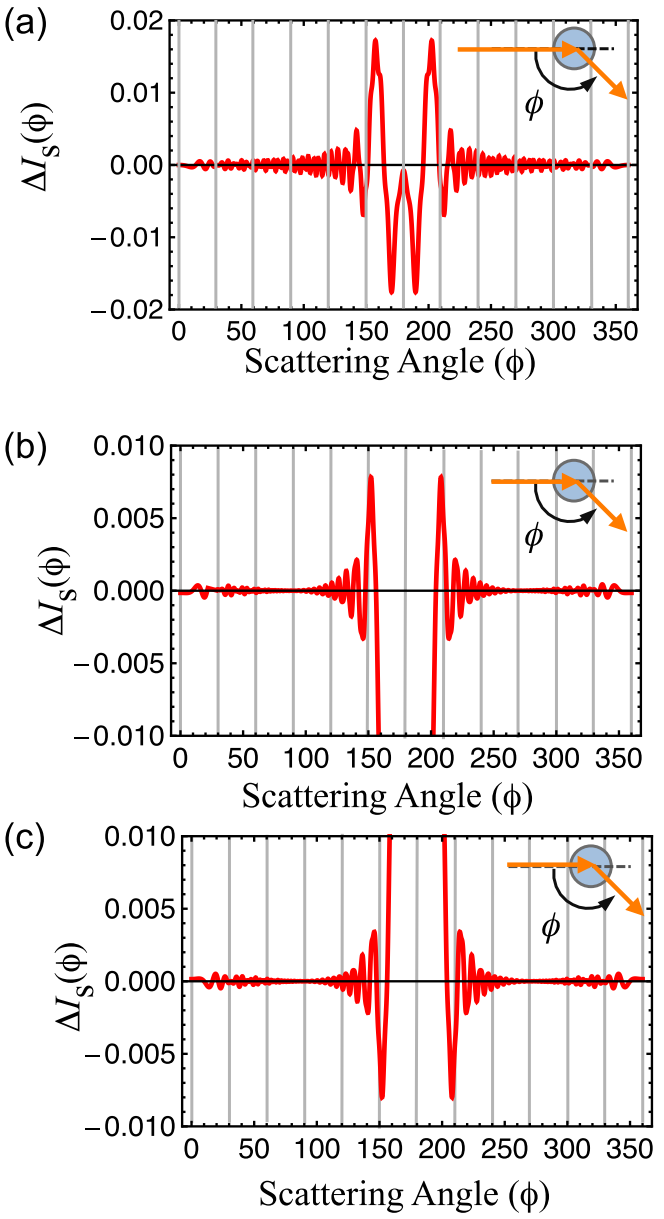

FIG. 10. (Color online) Calculated scattering intensity $I_s(\phi)$ from a cylinder with (a) $\Delta n = 0.001$ and $\kappa = 0$, (b) $\Delta n = 0$ and $\kappa = 0.001$, and (c) $\Delta n = 0$ and $\kappa = -0.001$, as a function of scattering angle ϕ.

the theoretical description in the literature [35,36]. The details of the RI evaluation are given in Appendix B. Because such a small RI difference and scattering efficiency (on the order of 10^{-2}) result in the random laser oscillation, the optical gain $\sim$300 cm^{-1} in the holes provides sufficient scattering efficiency for the random laser oscillation to occur. Therefore, we conclude that the random lasing originates in scattering due to the gain medium, even when the real part of the RI of the solution is close to that of the PCF.

IV. CONCLUSION

We report a random laser action in a holey PCF whose holes are filled with a DCM solution. Although the holes of the PCF

are periodically ordered, the observed laser action does not stem from the Bragg reflection due to the periodic structure and is ascribed to the multiple scattering by the holes.

We also show that a random laser may occur even when the real part of the RIs of the scatterers is equal to that of the surrounding medium, if the scatterers have optical gain. Because the optical gain is expressed by the negative imaginary part of the RI, a random laser with weak scatterers is possible.

The advantages of using PCFs instead of particles as a random laser platform are as follows: (1) the size distribution of the PCF holes is narrow, (2) a variety of scattering conditions can be examined using solutions with different RIs, and (3) the laser emission is confined mainly to the plane of incidence because of the PCF structure. Therefore it is a promising quasi-two-dimensional random laser platform that is convenient for investigating the mechanism of random-laser oscillation.

ACKNOWLEDGMENTS

This work was partially supported by a Grant-in-Aid for Scientific Research (Grants No. 25109707, No. 26600023, and No. 26286058) from the Japan Society for the Promotion of Science.

APPENDIX A: LIGHT SCATTERING BY A CYLINDER

Here we consider the problem of light scattering from a cylinder with a diameter a and infinite length as shown in Fig. 11. Cylindrical coordinates are used. The general expression is provided in the literature [26–28]. The RI of the cylinder is m_1. It is located in a medium with a RI of m_0. Light at an angular frequency ω with an amplitude E_0 and a vacuum wave number k_v is incident normal to the cylinder. We define the variables ρ_q and E_n as

$$\rho_q = r m_q k_\mathrm{v}, \tag{A1}$$

$$E_n = \frac{E_0(-i)^n}{k_q}, \tag{A2}$$

where n is an integer corresponding to the order of the Bessel $J_n(\rho_q)$ and Hankel $H_n(\rho_q)$ functions. $k_q = m_q k_\mathrm{v}$, where q identifies the medium and $q = 1$ or 2. The vector cylindrical harmonics are

$$\mathbf{M}_n = k_q\left(in\frac{Z_n(\rho_q)}{\rho_q}\hat{\mathbf{e}}_\mathbf{r} - Z_n'(\rho_q)\hat{\mathbf{e}}_\phi\right)e^{in\phi}, \tag{A3}$$

$$\mathbf{N}_n = k_q Z_n(\rho_q)\hat{\mathbf{e}}_\mathbf{z} e^{in\phi}, \tag{A4}$$

where $Z_n(\rho_q)$ is a Bessel or Hankel function of order n. $\hat{\mathbf{e}}_\mathbf{r}$, $\hat{\mathbf{e}}_\phi$, and $\hat{\mathbf{e}}_\mathbf{z}$ are unit vectors in the r, ϕ, and z directions, respectively. The prime indicates the differentiation by the argument in the parentheses.

In the TM polarization, the electric field of the incident light is $\mathbf{E}_\mathrm{i} = (0,0,E_{\mathrm{i}z})$, that of the cylinder is $\mathbf{E}_1 = (0,0,E_{1z})$, and that of the scattered light $\mathbf{E}_\mathrm{s} = (0,0,E_{\mathrm{s}z})$. The nonzero components are

$$E_{\mathrm{i}z} = E_0\sum_{n=-\infty}^{\infty}(-i)^n J_n(\rho_0)e^{in\phi}, \tag{A5}$$

$$E_{1z} = E_0\sum_{n=-\infty}^{\infty}(-i)^n f_n J_n(\rho_1)e^{in\phi}, \tag{A6}$$

$$E_{\mathrm{s}z} = -E_0\sum_{n=-\infty}^{\infty}(-i)^n b_n H_n(\rho_0)e^{in\phi}, \tag{A7}$$

where b_n and f_n are constants at an order n. The magnetic fields have two components: $\mathbf{H}_\mathrm{i} = (H_{\mathrm{i}r}, H_{\mathrm{i}\phi}, 0)$ in the incident light, $\mathbf{H}_1 = (H_{1r}, H_{1\phi}, 0)$ in the cylinder, and $\mathbf{H}_\mathrm{s} = (H_{\mathrm{s}r}, H_{\mathrm{s}\phi}, 0)$ in the scattered light. The ϕ components are

$$H_{\mathrm{i}\phi} = \frac{ik_0}{\omega\mu_0}E_0\sum_{n=-\infty}^{\infty}(-i)^n J_n'(\rho_0)e^{in\phi}, \tag{A8}$$

$$H_{1\phi} = \frac{ik_1}{\omega\mu_0}E_0\sum_{n=-\infty}^{\infty}(-i)^n f_n J_n'(\rho_1)e^{in\phi}, \tag{A9}$$

$$H_{\mathrm{s}\phi} = -\frac{ik_0}{\omega\mu_0}E_0\sum_{n=-\infty}^{\infty}(-i)^n b_n H_n'(\rho_0)e^{in\phi}, \tag{A10}$$

where μ_0 is the vacuum permeability.

The boundary condition at the cylinder surface, $E_{\mathrm{i}z} + E_{\mathrm{s}z} = E_{1z}$, $H_{\mathrm{i}\phi} + H_{\mathrm{s}\phi} = H_{1\phi}$, yields the following equations for b_n and f_n:

$$b_n = \frac{m_0 J_n(m_1x)J_n'(m_0x) - m_1 J_n'(m_1x)J_n(m_0x)}{m_0 J_n(m_1x)H_n'(m_0x) - m_1 J_n'(m_1x)H_n(m_0x)}, \tag{A11}$$

$$f_n = \frac{m_0 J_n(m_0x)H_n'(m_0x) - m_0 J_n'(m_0x)H_n(m_0x)}{m_0 J_n(m_1x)H_n'(m_0x) - m_1 J_n'(m_1x)H_n(m_0x)}, \tag{A12}$$

where x is the size parameter ($x = k_\mathrm{v}a$).

In the TE polarization, the electric field has two components: $\mathbf{E}_1 = (E_{1r}, E_{1\phi}, 0)$ in the incident light, $\mathbf{E}_1 = (E_{1\mathrm{r}}, E_{1\phi}, 0)$ in the cylinder, and $\mathbf{E}_\mathrm{s} = (E_{\mathrm{s}r}, E_{\mathrm{s}\phi}, 0)$ in the scattered light. The ϕ components are

$$E_{\mathrm{i}\phi} = iE_0\sum_{n=-\infty}^{\infty}(-i)^n J_n'(\rho_0)e^{in\phi}, \tag{A13}$$

$$E_{1\phi} = iE_0\sum_{n=-\infty}^{\infty}(-i)^n g_n J_n'(\rho_1)e^{in\phi}, \tag{A14}$$

$$E_{\mathrm{s}\phi} = -iE_0\sum_{n=-\infty}^{\infty}(-i)^n a_n H_n'(\rho_0)e^{in\phi}. \tag{A15}$$

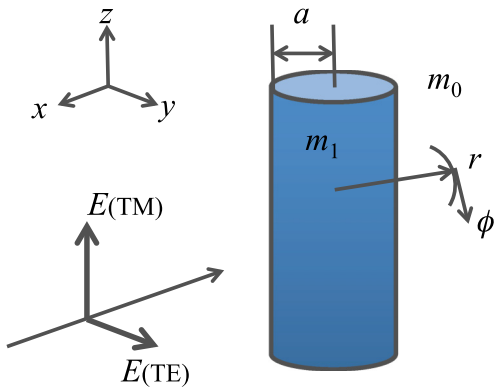

FIG. 11. (Color online) Geometry for the calculating of the scattering intensity from a cylinder of infinite length.

The corresponding magnetic fields are

$$H_{iz} = -\frac{ik_0}{\omega\mu_0} E_0 \sum_{n=-\infty}^{\infty} (-i)^n J_n(\rho_0) e^{in\phi}, \quad \text{(A16)}$$

$$H_{1z} = -\frac{ik_1}{\omega\mu_0} E_0 \sum_{n=-\infty}^{\infty} (-i)^n g_n J_n(\rho_1) e^{in\phi}, \quad \text{(A17)}$$

$$H_{sz} = \frac{ik_0}{\omega\mu_0} E_0 \sum_{n=-\infty}^{\infty} (-i)^n a_n H_n(\rho_0) e^{in\phi}. \quad \text{(A18)}$$

The constants a_n and g_n can be calculated from the boundary condition:

$$a_n = \frac{m_1 J_n'(m_0 x) J_n(m_1 x) - m_0 J_n(x_0) J_n'(m_1 x)}{m_1 J_n(m_1 x) H_n'(m_0 x) - m_0 J_n'(m_1 x) H_n(m_0 x)}, \quad \text{(A19)}$$

$$g_n = \frac{m_0 J_n(m_0 x) H_n'(m_0 x) - m_0 H_n(m_0 x) J_n'(m_0 x)}{m_1 J_n(m_1 x) H_n'(m_0 x) - m_0 J_n'(m_1 x) H_n(m_0 x)}. \quad \text{(A20)}$$

In the TM polarization, the electric fields of the incident and scattered light are reduced to

$$\mathbf{E}_i = E_0 \sum_{n=-\infty}^{\infty} (-i)^n J_n(\rho_0) e^{in\phi} \hat{\mathbf{e}}_\mathbf{z}, \quad \text{(A21)}$$

$$\mathbf{E}_s = -E_0 \sum_{n=-\infty}^{\infty} (-i)^n b_n H_n(\rho_0) \hat{\mathbf{e}}_\mathbf{z}. \quad \text{(A22)}$$

In the TE polarization, they are

$$\mathbf{E}_i = iE_0 \sum_{n=-\infty}^{\infty} (-i)^n J_n'(\rho_0) \hat{\mathbf{e}}_\phi, \quad \text{(A23)}$$

$$\mathbf{E}_s = -iE_0 \sum_{n=-\infty}^{\infty} (-i)^n a_n H_n'(\rho_0) \hat{\mathbf{e}}_\phi. \quad \text{(A24)}$$

We define the scattered light intensity $\Delta I_s(\phi)$ as the difference between $I_s(\phi)$ and $I_0(\phi)$:

$$\Delta I_s(\phi) = I_s(\phi) - I_0(\phi) = |E_s(\phi) + E_i(\phi)|^2 - |E_i(\phi)|^2. \quad \text{(A25)}$$

APPENDIX B: EVALUATION OF SPATIAL RI INHOMOGENEITY DUE TO THERMAL FLUCTUATION OF NLC

An NLC is cloudy because it scatters visible light, mainly because of thermal fluctuation of the director, that is, the pointing direction of the long axis of NLC molecules.

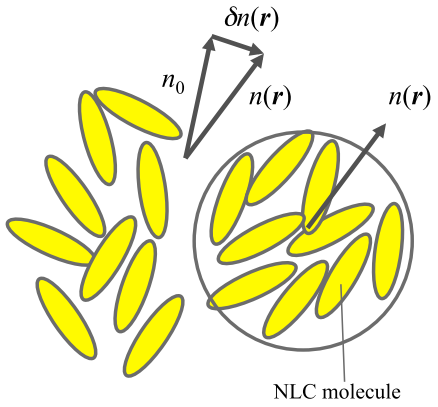

FIG. 12. (Color online) Schematic picture of NLC.

Consider the NLC as shown in Fig. 12. The average direction of ordering of the NLC molecules is called the "director" vector $\boldsymbol{n}_0$. The NLC is uniaxial and has the RI components of m_o (ordinary) and m_e (extraordinary). According to the equipartition of theorem [35,36], the Fourier component of fluctuation of the director, $\delta n(q)$, at wave number q is approximated to

$$[\delta n(q)]^2 = \frac{k_B T}{K q^2} \Omega, \quad \text{(B1)}$$

where K is the elastic constant of NLC, k_B is the Boltzmann constant, and T is temperature. Ω is a small volume to consider.

Because the dimensions of the scatterer are on the order of the light wavelength, $q \sim 10^6\ \mathrm{m}^{-1}$, $\delta n(q)$ is evaluated to be on the order of $10^{-21}\ \mathrm{m}^3$ using the parameters $k_B \sim 10^{-23}\ \mathrm{J\,K}^{-1}$, $T \sim 300$ K, and $K \sim 10^{-12}$ N. The volume Ω corresponding to the $q \sim 10^6\ \mathrm{m}^{-1}$ is on the order of $10^{-18}\ \mathrm{m}^3$.

The square of the degree of the fluctuation $\langle \sin^2\theta \rangle$ is

$$\langle \sin^2\theta \rangle \sim [\delta n(q)]^2/\Omega^2 = \frac{k_B T}{K q^2 \Omega} \sim 10^{-3}. \quad \text{(B2)}$$

Consequently, the RI fluctuation Δn due to the fluctuation is evaluated as follows:

$$\begin{aligned} \Delta n &= m_e m_o \left(m_e^2 \cos^2\theta + m_o^2 \sin^2\theta\right)^{-\frac{1}{2}} - m_e \\ &\sim m_e (1 + \sin^2\theta)^{-\frac{1}{2}} - m_e \\ &\sim m_e \left(1 - \tfrac{1}{2}\sin^2\theta\right) - m_e = -\tfrac{1}{2} m_e \sin^2\theta \\ &\sim 10^{-3} m_e. \end{aligned} \quad \text{(B3)}$$

[1] G. P. Berman, A. Lawandy, and J. F. M. Izrailev, Nature (London) **368**, 436 (1996).
[2] N. M. Lawandy, R. M. Balachandran, A. S. L. Gomes, and E. Sauvain, Nature (London) **368**, 436 (1994).
[3] D. S. Wiersma and A. Lagendijk, Phys. Rev. E **54**, 4256 (1996).
[4] H. Cao, Y. G. Zhao, S. T. Ho, E. W. Seelig, Q. H. Wang, and R. P. H. Chang, Phys. Rev. Lett. **82**, 2278 (1999).
[5] D. S. Wiersma and S. Cavalieri, Nature (London) **414**, 708 (2001).
[6] G. D. Dice, S. Mujumdar, and A. Y. Elezzabi, Appl. Phys. Lett. **86**, 131105 (2005).
[7] D. S. Wiersma, Nature Phys. **4**, 359 (2008).
[8] S. Ferjani, A. D. Luca, V. Barna, C. Versace, and G. Strangi, Opt. Express **17**, 2042 (2009).

[9] C.-R. Lee, J.-D. Lin, B.-Y. Huang, S.-H. Lin, T.-S. Mo, S.-Y. Huang, C.-T. Kuo, and H.-C. Yeh, Opt. Express **19**, 2391 (2011).
[10] D. S. Wiersma and S. Cavalieri, Phys. Rev. E **66**, 056612 (2002).
[11] F. Yao, W. Zhou, H. Bian, Y. Pei, X. Sun, and Z. Lv, Opt. Lett. **38**, 1557 (2013).
[12] X. Meng, K. Fujita, S. Murai, Y. Zong, S. Akasaka, H. Hasegawa, and K. Tanaka, Phys. Status Solidi C **6**, S102 (2009).
[13] S. M. Morris, D. J. Gardiner, M. M. Qasim, P. J. W. Hands, T. D. Wilkinson, and H. J. Coles, Appl. Phys. Lett. **111**, 033106 (2012).
[14] Y. Nagai, R. Fujimura, and K. Kajikawa, Jpn. J. Appl. Phys. **53**, 01AE05 (2014).
[15] C. J. S. de Matos, L. de S. Menezes, A. M. Brito-Silva, M. A. Martinez Gámez, A. S. L. Gomes, and C. B. de Araújo, Phys. Rev. Lett. **99**, 153903 (2007).
[16] J. C. Knight, T. A. Birks, P. S. J. Russell, and D. M. Atkin, Opt. Lett. **21**, 1547 (1996).
[17] J. C. Knight, Nature (London) **424**, 847 (2003).
[18] P. Russell, Science **299**, 358 (2003).
[19] J. Villatoro, M. P. Kreuzer, R. Jha, V. P. Minkovich, V. Finazzi, G. Badenes, and V. Pruneri, Opt. Express **17**, 1447 (2009).
[20] R. Jha, J. Villatoro, G. Badenes, and V. Pruneri, Opt. Lett. **34**, 617 (2009).
[21] www.newport.com.
[22] www.refractiveindex.info.
[23] J. C. Knight, H. S. Driver, and G. N. Robertson, Opt. Lett. **18**, 1296 (1993).
[24] H.-J. Moon and K. An, Appl. Phys. Lett. **80**, 3250 (2002).
[25] Y. Nagai, R. Fujimura, and K. Kajikawa, J. Opt. Soc. Am. B **30**, 2233 (2013).
[26] H. C. van de Hulst, *Light Scattering by Small Particles* (Dover, New York, 1957).
[27] J. A. Strattton, *Electromagnetic Theory* (McGraw-Hill, New York, 1941).
[28] C. F. Bohren and D. R. Huffman, *Absorption and Scattering of Light by Small Particles* (Wiley, New York, 1983), pp. 194–208.
[29] V. Bulovi, V. G. Kozlov, V. B. Khanfin, and S. R. Forrest, Science **279**, 553 (1998).
[30] N. Noginova, A. V. Yakim, J. Soimo, L. Gu, and M. A. Noginov, Phys. Rev. B **84**, 035447 (2011).
[31] J. Seidel, S. Grafstrom, and L. Eng, Phys. Rev. Lett. **94**, 177401 (2005).
[32] M. A. Noginov, G. Zhu, M. Mayy, B. A. Ritzo, N. Noginova, and V. A. Podolskiy, Phys. Rev. Lett. **101**, 226806 (2008).
[33] M. Leonetti, R. Sapienza, M. Ibisate, C. Conti, and C. Lopez, Opt. Lett. **34**, 3764 (2009).
[34] U. Ganiel, A. Hardy, G. Neumaw, and D. Treves, IEEE J. Quantum Electron. **11**, 881 (1975).
[35] P. G. de Gennes and J. Prost, *The Physics of Liquid Crystals* (Oxford University Press, New York, 1993), pp. 139–150.
[36] S. Chandrasekhar, *Liquid Crystals* (Cambridge University Press, Cambridge, 1992), pp. 167–177.